# Multibunch Instabilities

Flemming Pedersen

CERN, Geneva, Switzerland

## 1 Introduction and Summary

The theory for transverse and longitudinal multibunch instabilities is reviewed. The coherent beam modes are classified, and the various mode numbers defining the coherent modes are explained. Sacherer's longitudinal and transverse growth rate formulae are discussed and compared with the commonly used short-bunch approximation and Robinson's characteristic equation. Coupling impedances with long-range wakes are particular troublesome for the large high-current colliders planned for the next decade. These are the higher-order modes of the RF cavities, the fundamental mode of the RF cavities, and the transverse resistive wall impedance.

**Table 1.** Classification of coherent beam modes

| | Coasting Beams | Bunched Beams |
|---|---|---|
| Longitudinal | $n$ = azimuthal mode number = 1,2,3, ... $\infty$ | $n$ = coupled bunch mode number = 0, 1, 2, ... ($M$-1)<br>$m$ = phase plane periodicity = 1 (dipole), 2 (quadrupole), 3 (sextupole), ...<br>($q$ = radial mode number) |
| | | Mode coupling $\Rightarrow$ Single-bunch "microwave" instability (turbulence). |
| Transverse | $n$ = azimuthal mode number = -$\infty$, ..., -1, 0, 1, 2, ... +$\infty$<br>$k$ = phase plane periodicity = 1 (dipole), 2 (quadrupole), 3 (sextupole), ... | $n$ = coupled bunch mode number = 0, 1, 2, ... ($M$-1)<br>$m$ = head-tail mode number = ..., -2, -1, 0 1, 2, ...<br>$k$ = phase plane periodicity = 1 (dipole), 2 (quadrupole), 3 (sextupole), .. |
| | | Mode coupling $\Rightarrow$ Single-bunch, fast, head-tail instability (turbulence). |

## 2 Classification of Coherent Beam Modes

Coherent beam modes are classified according to whether the coherent beam motion is longitudinal or transverse, and according to whether the beam is bunched or debunched (coasting beam), Table 1. In this way four main classes of coherent beam modes are defined. Beams are of course always bunched in e+/e- rings due to synchrotron radiation, but it is useful to classify the beam modes in this general way.

The complexity of the beam motion increases from longitudinal to transverse, and from coasting to bunched, such that the mode description requires an increasing number of mode numbers.

## 3 Longitudinal Bunched-Beam Modes

The general theory for coherent bunched beam modes and their interaction with the environment is due to Sacherer [1][2][3]. Basically two mode numbers describe the motion (see Fig. 1). The *coupled bunch mode number n* is defined as the *number of waves of coherent motion per revolution*, and resembles therefore the azimuthal mode number for coasting beams.

For bunched beams with $M$ equidistant bunches, the bunch-to-bunch phase shift $\Delta\phi$ is related to the coupled bunch mode number $n$ by $\Delta\phi = 2\pi n/M$. There are $M$ coupled bunch modes numbered from 0 to ($M$-1). This is in contrast to the azimuthal mode number for coasting beams, where there is an infinite number of modes.

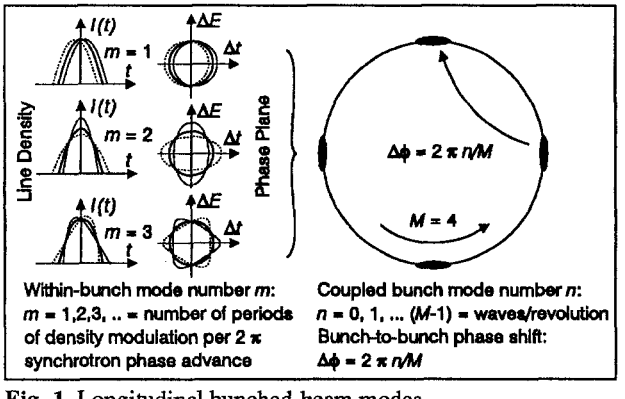


**Fig. 1.** Longitudinal bunched-beam modes

The within-bunch mode number $m$ is the *number of periods of phase space density modulation per synchrotron period* in the longitudinal phase plane. The lowest mode number is $m = 1$, which corresponds to the dipole mode, $m = 2$ is the quadrupole mode, $m = 3$ is the sextupole mode and so on. The line density is the projection of the phase space distribution on the time axis. The observed pattern for a given bunch oscillates with $m$ times the synchrotron frequency, and the pattern has $m$ nodes along the bunch (see Fig. 1).

The theory for longitudinal bunched beam mode interactions [4][5] contains in addition a *radial mode number* $q = m, m+2, \ldots$, which is describing an infinity of orthogonal radial modes with different density variations versus synchrotron amplitude (= radius). The first higher-order radial mode $q = 3$ for the dipole mode

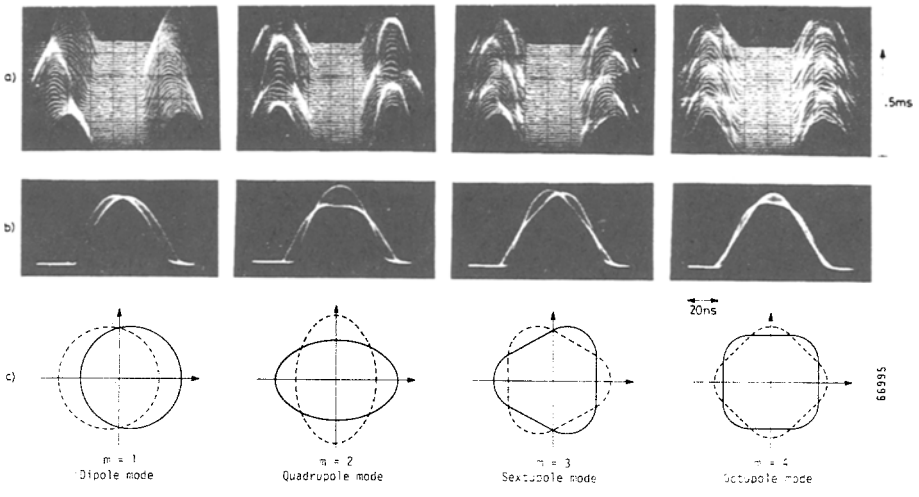


**Fig. 2.** Within bunch modes $m = 1$ to 4, coupled-bunch pattern $n = 4$. a) Mountain-range display of one synchrotron period; b) Superimposed; c) Phase space.

($m = 1$) has thus a line density pattern which looks like a sextupole mode ($m = 3$), but it oscillates with the synchrotron frequency and not three times this frequency. Normally only the lowest radial mode is observed. This is probably due to the fact that the higher radial modes have higher Landau damping thresholds [5].

An example of various different coupled bunch modes observed in the CERN PS Booster ($M = 5$, $n = 4$, $m = 1$ to 4) is shown on Fig. 2. Note the bunch-to-bunch phase shift of the coherent motion of $\Delta\phi = 360°*n/M = 288° = -72°$.

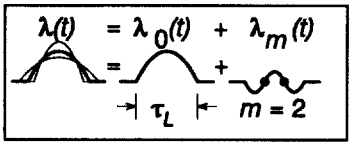


**Fig. 3.** Stationary and oscillating part of line density

It is apparent from figures 1 and 2 that the line density $\lambda(t)$ or current $I(t) = e\,\lambda(t)$ of a bunch can be decomposed into two parts, the stationary distribution $\lambda_0(t)$ plus an additional charge density $\lambda_m(t)$ oscillating at $m$ times the synchrotron frequency. The oscillating part $\lambda_m(t)$ is an approximately sinusoidal standing-wave pattern with $m$ fixed nodes along the bunch (Fig. 3).

By taking the Fourier transform of the bunch current $I(t)$, we get the frequency spectrum of the modes. It is a line spectrum, and the line frequencies for mode $(n,m)$ are:

$$f_{nm,p} = (n + pM)f_0 + mf_s \quad -\infty < p < +\infty \tag{1}$$

where $f_0$ is the revolution frequency, $f_s$ is the synchrotron frequency, and $p$ is an integer assuming both negative and positive values. It is convenient from a mathematical point of view to let the frequencies $f_{nm,p}$ assume both positive and negative values, although physically a frequency is always a positive quantity.

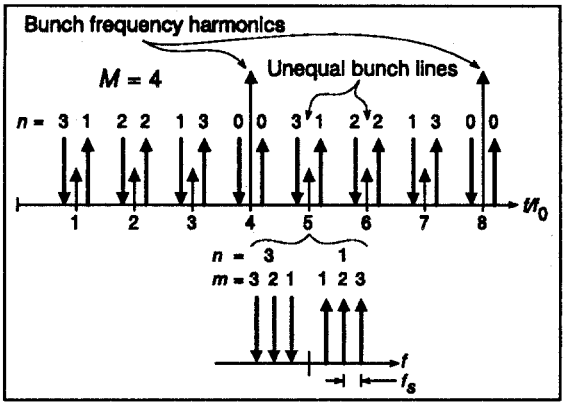


**Fig. 4.** The line spectrum of longitudinal bunched beam modes

This line spectrum is depicted graphically (see Fig 4), where the mode lines originating from negative values of $f_{nm,p}$ (lower sidebands) are shown as downward pointing arrows, while mode lines originating from positive values (upper sidebands) are shown pointing up. The spectral lines given by equation (1) are those associated with the coherent motion or the oscillating part of the bunch $\lambda_m(t)$. In addition there are lines associated with the stationary bunch spectrum or $\lambda_0(t)$. There are strong lines at the bunch frequency $Mf_0$ and harmonics thereof. In practice the $M$ bunches will have slightly different intensities or there might be a gap in the bunch train, which causes spectral lines of lower amplitude to appear at the intermediate revolution harmonics.

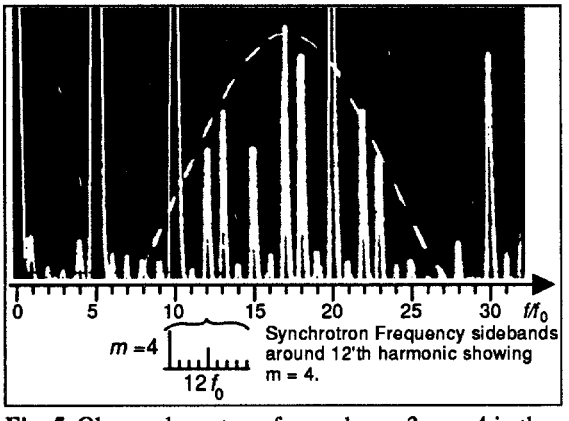


**Fig. 5.** Observed spectrum for mode $n = 3$, $m = 4$ in the CERN PSB. Bandwidth 300 kHz, range 0 - 50 MHz, linear scale, bunch length $\tau_L = 66$ ns.

Each bunched beam mode $(m,n)$ has thus two lines appearing within each band $Mf_0$ wide between two bunch frequency harmonics, one pointing up and one pointing down. Each mode has therefore a large number of spectral lines. The envelope or the relative amplitude of those lines depends upon the within-bunch mode number $m$ and the bunch length $\tau_L$.

An example of a measured longitudinal mode spectrum from the CERN PS Booster [3] is shown on Fig. 5 ($M = 5$, $n = 3$, $m = 4$, octupole mode). Both coherent mode lines, bunch frequency harmonics, and unequal bunch lines are clearly seen.

### 3.1 Sacherer's Formula for Longitudinal Bunched Beam Modes

Due to electromagnetic interactions with the beam environment quantitatively described by the longitudinal coupling impedance $Z_L(\omega)$, the coherent mode

frequencies are shifted a complex quantity $\Delta\omega_{mn}$ away from their low intensity values. This shift is obtained by a weighted sum (factor $F_m(f_p\tau_L)$) of the coupling impedance $Z_L(\omega_p)$ sampled at all those frequencies $\omega_p = 2\pi f_p$ that corresponds to a mode line (see Fig. 4, equation (1)) of mode $(m,n)$, Sacherer's formula [1][2][3]:

$$\Delta\omega_{mn} = j\omega_s \frac{m}{m+1} \frac{I}{3B_0^2 hV\cos\phi_s} \sum_p F_m(f_p\,\tau_L) \frac{Z_L(f_p)}{p+n} \tag{2}$$

where $\omega_s$ is the synchrotron frequency, $I$ is the total beam current in $M$ bunches, $B_0$ the bunching factor ($= \tau_L/T_0$, where $T_0 = 1/f_0$ is the revolution period), $h$ the harmonic number, $V$ the total RF voltage, $\phi_s$ is the synchronous phase angle with the convention that $V\sin\phi_s$ is the energy gain per turn, $\phi_s < 90°$ below transition, $\phi_s > 90°$ above transition, and $\tau_L$ the full bunch length. The form factor $F_m$ is the normalised power spectrum of the perturbed part $\lambda_m(t)$ of the line density $\lambda(t)$:

$$F_m(f_p\tau_L) = \frac{1}{MB_0} \frac{\left|\tilde{\lambda}_m(p)\right|^2}{\sum_p \left|\tilde{\lambda}_m(p)\right|^2} \tag{3}$$

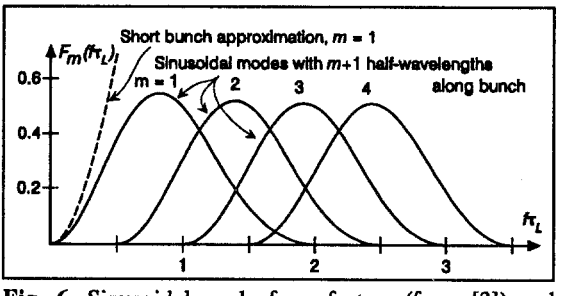


**Fig. 6.** Sinusoidal mode form factors (from [3]) and short bunch approximation

where $\tilde{\lambda}_m(p)$ is the Fourier transform of the perturbed part $\lambda_m(t)$ of the line density and $M$ the number of equidistant bunches. For the sinusoidal type modes shown on Fig. 3, the form factors $F_m(f\tau_L)$ are plotted on Fig. 6.

The *growth rate* of mode $(m,n)$ is $-\mathrm{Im}\{\Delta\omega_{mn}\}$ which is related to the *real* part of the coupling impedance $Z_L(\omega)$. The *real coherent frequency shift* of mode $(m,n)$ is $\mathrm{Re}\{\Delta\omega_{mn}\}$, which is related to the *imaginary* part of the coupling impedance.

### 3.2 Discussion of Sacherer's Longitudinal Bunched Beam Formula

The real part of the coupling impedance $Z_L(\omega)$ is symmetric, ($\mathrm{Re}\{Z_L(\omega)\} = \mathrm{Re}\{Z_L(-\omega)\}$), so contributions to the sum in (2) associated with negative and positive values of $f_p$ (mode lines pointing down and up on Fig. 4) enter with opposite signs due to the factor $1/(p+n)$. Broad-band and resonant impedances with bandwidths larger than the bunch frequency $Mf_0$ (decay time less than bunch separation) do therefore not cause any growth or damping rate. Each mode has two mode lines in each band between two bunch frequency harmonics, and their contributions to the sum of (2) tend to cancel each other.

For resonant impedances with bandwidths smaller than the bunch frequency $Mf_0$ (decay time longer than bunch separation), a single mode line for each mode dominates in the sum and one or several coupled-bunch modes grow. The growth rate is proportional to the total current $I$ in $M$ bunches, and independent of the number of bunches unless the bunch frequency is low enough to get partial cancellation from another mode line of the same mode falling within the resonator bandwidth.

The signs in (2) are such that *upper* sidebands are *unstable above* transition, and lower sidebands are stable (assuming *passive* coupling impedances: $\mathrm{Re}\{Z_L\} > 0$). The opposite is true below transition. For $M \geq 3$ upper and lower sidebands belong to different coupled-bunch modes (except for $n = 0$ and $M/2$) so a resonator will drive one mode $n_1$ and damp the other complementary mode $n_1$-$M$. For a single bunch, or two bunches, upper and lower sidebands belong to the same coupled-bunch mode and therefore tend to cancel unless the impedance is very narrow-band (such as the fundamental RF resonance) and tuned asymmetrically with respect to the frequencies with mirror symmetry such as $pMf_0$ or $(p+½)Mf_0$.

The imaginary part of the coupling impedance $Z_L(\omega)$ is anti symmetric, $(\mathrm{Im}\{Z_L(\omega)\} = -\mathrm{Im}\{Z_L(-\omega)\}$, so contributions to the sum in (2) associated with negative and positive values of $f_p$ (mode lines pointing down and up on Fig. 4) add up, so even a broad-band impedance can produce a substantial real frequency shift due to its imaginary part. For the special case of inductive-wall or space-charge impedance, where $\mathrm{Im}\{Z_L(\omega_p)/p\}$ is constant below a certain frequency, we can move $Z_L(\omega_p)/p$ outside the summation, and we get for the real coherent frequency shift:

$$\Delta\omega_{1n} = -\omega_s \frac{I}{6B_0^3 MhV\cos\phi_s} \mathrm{Im}\{\frac{Z_L}{p}\} \tag{4}$$

This is the coherent shift relative to the incoherent frequency $\omega_s$ as given by the total voltage $V$ *including* the inductive-wall contribution itself. The expression agrees with the expression given in [6] except for a factor $(\pi/3)^2 = 1.097$. It is a single-bunch, short-range wake effect where all coupled-bunch modes $n$ have the same shift, which is the same as saying that all individual bunches have their coherent frequencies shifted the same amount. As expected, the shift is proportional to the current per bunch $I/M$.

### 3.3 Turbulent Bunch Lengthening and Longitudinal Mode Coupling

For sufficiently high currents (or sufficiently high impedances), single bunches can become unstable, as was first observed by Boussard [7]. The instability is usually called the microwave instability in proton rings due to the high frequencies involved, or turbulent bunch lengthening in electron rings, probably due to difficulties involved in observing the even higher frequencies involved in electron rings. The instability threshold is given by the Keil-Schnell criterion [8] for coasting beams, but with local values of bunch current and momentum spread as suggested by Boussard.

It was shown by Sacherer [2], that this threshold is consistent with the mode coupling threshold for two higher order longitudinal modes $m$ and $m$+1, as the real frequency shifts associated with the imaginary part of the coupling impedance cause their frequencies to cross. The mode coupling theory gives a more precise information about the threshold dependence upon resonator bandwidth than the Boussard criterion.

### 3.4 Short Bunch Approximation for Dipole Modes

Bunches in e+/e- rings are often so short that the frequencies of interest below the vacuum pipe cut-off frequency are below the peak of $F_1$. In this case the complex coherent frequency shift for the dipole mode $m = 1$ can be simplified to:

$$\Delta\omega_{1,n} = -j\frac{I\eta}{2Q_s\beta^2(E/e)}\sum_p f_p Z_L(f_p) \tag{5}$$

where $\eta = 1/\gamma_t^2 - 1/\gamma^2$, $I$ is the total beam current, $Q_s = \omega_s/\omega_0$ is the longitudinal tune, $E$ is the total energy, $e$ the fundamental charge, $\beta$ and $\gamma$ the usual relativistic parameters, and $\gamma_t$ is the transition energy. Note that the form factor $F_1$ does not appear in this equation. By using the expression for the synchrotron frequency $\omega_s$:

$$\omega_s = \omega_0\sqrt{\frac{-\eta h V\cos\phi_s}{2\pi(E/e)\beta^2}} \tag{6}$$

and equating the coherent shifts given by equation (5) and (2) we get an expression for the rigid dipole mode form factor $F_1$ implied in equation (5):

$$F_1(f\tau_L) = 3(p+n)^2 B_0^2 = 3(f\tau_L)^2 \tag{7}$$

which is plotted on Fig. 6 together with the form factor for the sinusoidal modes. It corresponds to the initial parabolic behaviour of $F_1(f\tau_L)$, and is a valid approximation for $f\tau_L << 0.5$.

It is seen from Fig. 6, that the form factor corresponding to the short bunch formula (5) is slightly higher than the form factor computed from sinusoidal modes. This is because the sinusoidal modes assumed are slightly different from the rigid bunch motion assumed in (5).

## 4 Longitudinal Coupling Impedances

Longitudinal coupling impedances can be subdivided into *short-range-wake or broad-band* impedances (bandwidth > $Mf_0$), which have identical effects on all bunches and on all coupled-bunch modes $n$, and *long range wake or narrow band* impedances (bandwidth < $Mf_0$) which have very different effects on the different coupled bunch modes $n$ due to the line structure of the spectrum. Note that the

dividing criterion depends on the bunch frequency $Mf_0$ or bunch separation $1/Mf_0$, since the crucial point is whether the wake decays in the bunch interval.

Broad-band impedances are responsible for single-bunch effects, which have thresholds related to current per bunch, and where each bunch behaves independently of the others. Narrow-band impedances are responsible for multibunch effects, where the thresholds are related to total current, and the coupled-bunch mode number is important.

Next generation, high-current colliders (B, tau/charm and phi factories) typically have very high bunch frequencies, and even fairly well damped broad band resonators have significant long-range multibunch effects.

### 4.1 Parasitic Higher Order Modes

RF cavities are often the major source of long-range, narrow-band coupling impedances due to undesired higher-order modes (HOM's) between the fundamental RF resonance and the vacuum pipe cut-off frequency. For low total current and low bunch frequencies, it is usually possible to lower the Q and the shunt impedance of these cavities to a level where the coupled-bunch growth rates are below the synchrotron radiation damping rate.

For high-current colliders, sophisticated HOM damping schemes [9] are required to damp the higher-order modes by more than two orders of magnitude without significantly affecting the fundamental mode. Usually one or several wave guides with a cut-off frequency between the fundamental RF cavity resonance and the lowest frequency higher-order mode form a high-pass filter between the RF cavity and the HOM loads, both for normal conducting cavities [10][11] and superconducting cavities [12], where an enlarged portion of the beam pipe is used as a HOM wave guide.

Even with a sophisticated HOM damping scheme, the residual shunt impedance may still be large enough to cause longitudinal dipole-mode growth rates in excess of the synchrotron radiation damping rate, and a multibunch feedback system is required to stabilise all the modes. Operating with a high RF voltage, as required to obtain short bunches, appears to make the growth rate smaller ($\omega_s^{-1}$ scaling, equation (5)), but does in fact make it worse, as the total resonant HOM impedance $Z_L$ is proportional to the number of cavities.

If the bandwidth of the HOM's is large compared with the synchrotron frequency, about half the coupled-bunch modes are unstable as discussed above. For one or two bunches growth rates are small due to cancellation, since upper and lower sidebands at each harmonic belong to the same mode $n$. For small rings with high synchrotron tune and little or no HOM damping, the HOM bandwidths may become small compared to the synchrotron frequency, and cancellation is no longer effective. This is the case for the SLC damping rings [13], where HOM's of the accelerating cavities drive the $n = 1$ mode ($M = 2$), also called the $\pi$ mode, unstable. This fact can also be used with advantage to passively damp the instability. The instability has been cured by *adding* a passive cavity, tuned to interact mainly with the a lower sideband of the $n = 1$ mode.

## 4.2 Fundamental Resonance of RF Cavities

For small rings, the fundamental resonance interacts only with the $n = 0$ mode, which is easily stabilised (at least for electron rings with no complex RF feedback loops) by an appropriate tuning of the RF cavity. For large rings with high beam currents, other coupled-bunch dipole modes ($n = M - 1$, $M - 2$, etc.) may be driven unstable.

### 4.2.1 The Robinson Criterion and the $n = 0$, $m = 1$ Mode

A complete analysis of the stability of the interaction between the $n = 0$ dipole mode of the beam and the fundamental resonance of the RF cavity (without feedback) was first described by Robinson [14], and results in a characteristic equation of fourth order. The stability criterion can be solved analytically, and above transition we get:

$$\frac{2I_0 \cos\phi_s}{I_B} < \sin 2\phi_z < 0 \tag{8}$$

where $I_0$ is the peak value of RF current required to drive the cavity to the operating voltage when in tune (the loss current), $I_B \cong 2\,I$ is the peak value of the fundamental RF component of the beam current, which for short bunches equals twice the beam DC current $I$, and $\phi_Z$ the impedance angle of the cavity impedance at the operating RF frequency. The notation used here is slightly different from the one used in Robinson's original paper. The two regions of instability corresponding to the two inequalities in (8) are depicted graphically on Fig. 7.

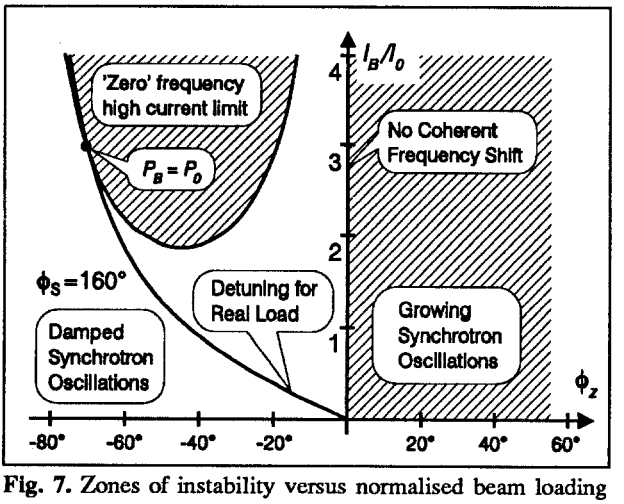


**Fig. 7.** Zones of instability versus normalised beam loading $I_B/I_0$, and cavity impedance angle $\phi_Z = \mathrm{Arg}(Z_L)$

For low currents the growth rate that is obtained from Robinson's characteristic equation by a root perturbation technique is in perfect agreement with the short bunch formula (5). If the cavity is tuned exactly to the operating RF frequency, the symmetry in the real part of the cavity impedance causes a perfect cancellation of the contributions from upper and lower sidebands, so no growth rate is induced of the $n = 0$, $m = 1$ mode. Since the imaginary part of the impedance is anti symmetric around the RF frequency, there is no real frequency shift either. By *detuning the cavity below the operating RF*

*frequency* (above transition) this mode is damped. This corresponds to satisfying the right hand inequality in (8).

Since the fundamental of the beam current is out of phase with the voltage, the beam load represents a partly reactive load to the RF source, which results in an unnecessary increased power demand from the RF source. By detuning the RF cavity such that a *real total load* (beam plus cavity) is presented to the RF source, less power is needed. This optimum detuning is usually done automatically by a tuning loop. It is fortunate that the signs are such that this detuning is always to the same side as that which produces damping of the $n = 0$ mode. At high current a *zero-frequency instability occurs* even if the cavity is detuned to the 'stable' side. This instability threshold corresponds to the left hand side of the Robinson criterion (8). This instability occurs (for optimum detuning) when the *beam power* equals or exceeds the *dissipated power* in the cavity (including the equivalent loss in the RF source impedance). If the power source is *back matched* (e. g. circulator in transmission line), the RF power source is *matched to the total load* (beam plus cavity), and the *cavity optimally detuned* (real total load) the system is in principle always stable against small transients, although not by a large margin if the beam power is significant.

The stability margin can be increased by increasing the detuning beyond optimum detuning, and by adjusting the power source to cavity RF coupling above optimum coupling (overcoupling).

### 4.2.2 Coupled Bunch Modes $n \neq 0$ Driven by the Detuned Fundamental Resonance

As mentioned above, it is essential to detune the cavity to compensate for the reactive part of the beam load to minimise the required RF power. The optimum detuning $\Delta f_{do}$ normalised to the revolution frequency $f_0$ is given by:

$$\frac{\Delta f_{do}}{f_0} = \frac{I_B \cos\phi_s}{2V_C}\left(\frac{R}{Q}\right)h \qquad (9)$$

where $I_B \cong 2I$ is the peak value of the fundamental RF component of the beam current, $V_C$ is the cavity voltage per cell, $\phi_s$ is the synchronous phase angle as previously defined, $R/Q$ is the shunt impedance over quality factor of a cavity cell (using the usual electrical engineering convention where $P = V_C^2/(2R)$), and $h$ the harmonic number. This value has been calculated for a number of medium to large high-current synchrotrons (Table 2). All of these rings are at present either in the design stage or under construction.

The fundamental RF resonance is likely to create a serious instability problem for the $n = M - 1, M - 2, ..$ modes if the cavity detuning is in the same order of magnitude as the revolution frequency or larger. It is seen from equation (9) that this is likely to happen for large $h$ (large ring, high RF frequency), high $R/Q$ value (low stored energy), high beam current, and at low voltage per cell. Using superconducting cavities, which have a high voltage per cell and a low $R/Q$, tend to

**Table 2.** Normalised optimum detuning for reactive beam load compensation

| Machine | $I_B[A_p]$ | $V_C$ [$kV_p$] | $R/Q$ [Ω] | $h$ | $\Delta f_{do}/f_0$ |
|---|---|---|---|---|---|
| PEP II | 4.28 | 925 | 117 | 3'492 | 0.93 |
| CESR B | 3.96 | 3000 | 45 | 1'275 | 0.038 |
| KEK B-fact. n/c | 5.2 | 390 | 98 | 5'120 | 3.34 |
| KEK B-fact. s/c | 5.2 | 2750 | 43 | 5'120 | 0.21 |
| SSC collider | 0.14 | 500 | 125 | 104'544 | 1.77 |
| SSC HEB | 0.90 | 325 | 150 | 2'178 | 0.45 |
| LHC | 1.70 | 1500 | 43 | 36'540 | 0.89 |
| KAON C | 5.6 | 100 | 100 | 225 | 0.63 |
| KAON D | 5.6 | 50 | 100 | 225 | 1.26 |

reduce the problem as is apparent from the three rings in the table above with superconducting cavities (CESR B, KEK s/c, and LHC). This also helps to solve problems associated with transients induced by beam gaps [15].

The growth rate can be very large. For the PEP II LER (low energy ring) for example it is the same order of magnitude as the synchrotron frequency, and almost three orders of magnitude larger than the radiation damping rate.

An obvious solution to the coupled-bunch problem would be not to detune the cavities, such that the cavity impedance is symmetric around the RF frequency. In most cases with heavy beam loading, the required extra RF power due to the large amounts of reflected power makes this solution unattractive. In addition the stable zone near the $\phi_z = 0$ axis is very narrow (Fig. 7), and the required tuning tolerances difficult to achieve, as a rather precise RF vector sum representing the total RF current injected into the cavity must be made.

Reducing the shunt impedance by loading, as used for the parasitic higher-order modes, is also totally unacceptable due to large amounts of wasted power. The most attractive solution is to apply RF cavity feedback [16][17][18], by which the apparent beam impedance of the RF system can be reduced several orders of magnitude.

Another solution being considered for the KEK B factory is to substantially lower the $R/Q$ of a normal conducting cavity by coupling it to a storage cavity operating in a very high $Q$ mode such that the lower $R/Q$ is achieved without much loss in shunt impedance [19].

## 5 Transverse Bunched-Beam Modes

The theory for the transverse coherent bunched-beam modes (Table 1, Fig. 8) and their interactions with the environment were again first described in its most general form by Sacherer [20][21]. As in the longitudinal case there are $M$ coupled bunch modes characterised by the *integer number of waves n of the coherent bunch motion around the ring*. The coupled-bunch mode number therefore resembles the azimuthal mode number $n$ for coasting beams.

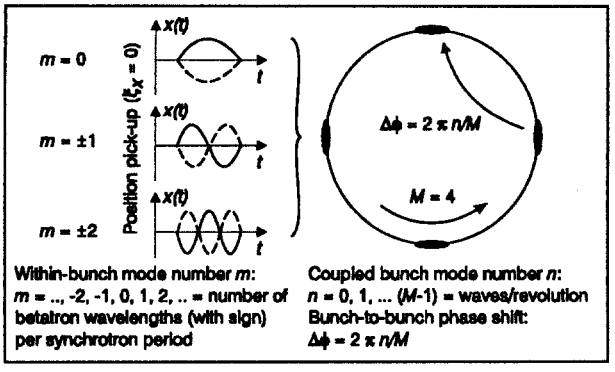


**Fig. 8.** Transverse bunched beam modes.

For bunched beams with $M$ equidistant bunches, the bunch-to-bunch phase shift $\Delta\phi$ is related to the coupled-bunch mode number $n$ by $\Delta\phi = 2\pi n/M$. There are $M$ coupled-bunch modes numbered from 0 to $(M\text{-}1)$. This is in contrast to the azimuthal mode number for coasting beams, where there is an infinite number of modes.

The within-bunch mode number $m$ (also called the *head-tail mode number*) is the net *number of betatron wavelengths (with sign) per synchrotron period* at a given instant. At any given instant, a closed pattern of $|m|$ betatron periods corresponds to one synchrotron period with the betatron phase either advancing ($m > 0$) or retarding ($m < 0$) in the direction of advancing synchrotron phase. Unlike the longitudinal case the mode number $m$ can thus assume both positive and negative integer values as well as zero. For $m = 0$ all particles in the bunch have the same betatron phase for zero chromaticity. The relation between longitudinal phase space co-ordinates ($\Delta E$, $\Delta t$) and transverse motion is depicted for zero chromaticity on the 3-D surface plots on Figs. 9 and 10, as well as the directly observable average displacement along the bunch.

There are $|m|$ nodes along the bunch. The transverse displacements for various energies at those positions along the bunch continue to average out to zero, so no

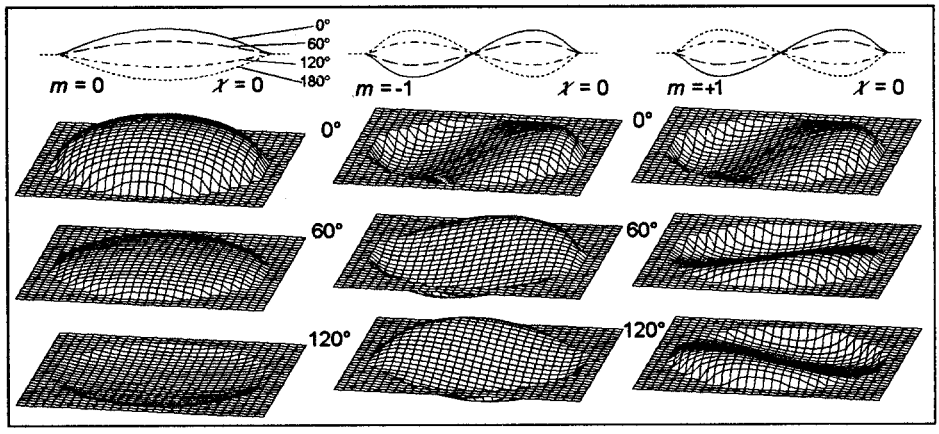


**Fig. 9.** Modes $m = 0$, -1, +1 for zero chromaticity. Surface plots indicating *transverse displacement times particle density* in longitudinal phase plane as function of longitudinal phase space co-ordinates $\Delta t$ (left/right), and $\Delta E$ (front/back) for three successive values of betatron phase. Top trace is average transverse displacement times line density as observed by the Δ-signal of a transverse pick-up.

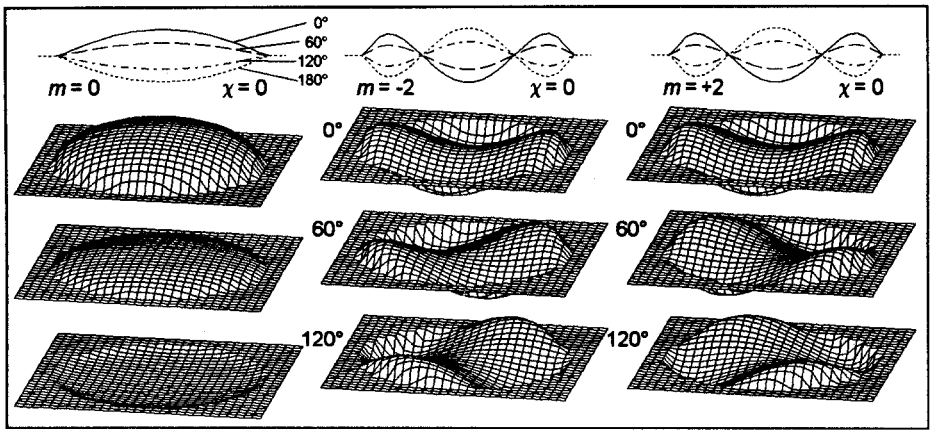


**Fig. 10.** Modes $m = 0, -2, +2$ for zero chromaticity

average displacement is observed on a pick-up, although there is much coherent transverse motion at different energies. The betatron phase pattern in the longitudinal phase plane appears to rotate either clockwise or counter-clockwise depending upon the sign of $m$. These two different senses of rotation are not immediately apparent from the observable, projected distribution, as they appear identical for mode $m = +1$, and mode $m = -1$. The difference is however apparent in the frequency domain, since the corresponding mode lines have slightly different frequencies, as the synchrotron frequency in one case is added to the betatron frequency, and in the other case subtracted.

For non-zero chromaticity $\xi$ there is a tune modulation $\Delta Q$ associated with the momentum modulation $\Delta p$ as a particle moves around the synchrotron orbit given by:

$$\frac{\Delta Q}{Q} = \xi \frac{\Delta p}{p} \tag{10}$$

This tune modulation results in a betatron phase advance $\chi$ during one half of the synchrotron period as the particle moves from head to tail of the bunch. This is compensated by a betatron phase retard $-\chi$ during the other half of the synchrotron period as the particle moves back from tail to head. The head-tail phase advance is proportional to the synchrotron amplitude and has its largest value for a particle with a synchrotron amplitude corresponding to the bunch length $\tau_L$, and is given by

$$\chi = \frac{\xi}{\eta} Q \omega_0 \tau_L \tag{11}$$

where $\eta = 1/\gamma_t^2 - 1/\gamma^2$, $\xi$ is the chromaticity as defined above, and $\omega_0$ is the revolution frequency

This chromaticity dependent phase modulation is then superimposed upon the betatron phase pattern given by the mode number $m$, see Fig. 11. It is seen that the average transverse displacement signal contains the same $|m|$ nodes as with zero

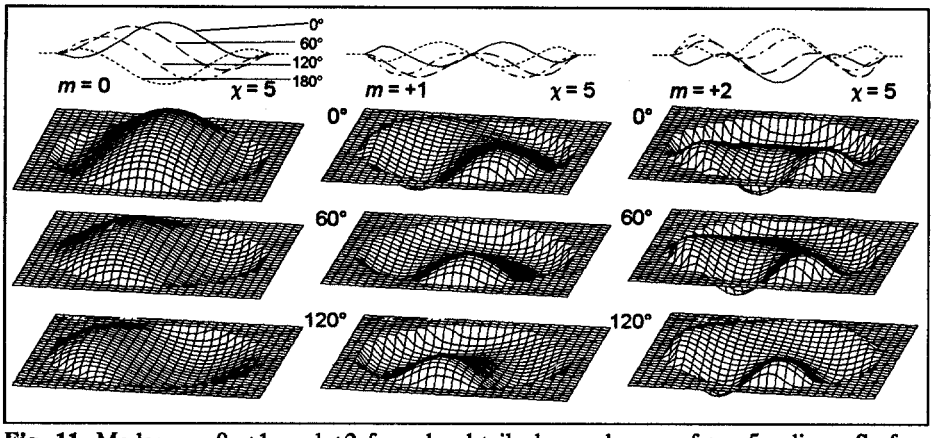


**Fig. 11.** Modes $m = 0$, +1, and +2 for a head-tail phase advance of $\chi = 5$ radians. Surface plots indicating *transverse displacement times particle density* in longitudinal phase plane as function of longitudinal phase space co-ordinates $\Delta t$ (left/right), and $\Delta E$ (front/back) for three successive values of betatron phase. Top trace is average transverse displacement times line density as observed by the Δ-signal of a transverse pick-up.

chromaticity, and that a travelling-wave component is added to the standing-wave patterns observed for zero chromaticity.

Average transverse displacements superimposed and turn by turn mountain range displays are shown on Fig. 13 for three different chromaticities and for modes $m = 0$, +1, and +2. An example of several different vertical bunched-beam modes observed in the CERN PSB is shown on Fig. 12.

In addition (see Table 1) there is a third mode number $k = 1$ (dipole), 2 (quadrupole), 3 (sextupole), etc. which is the *number of periods of density modulation per betatron period*. In general, and as assumed in the preceding discussion, the dipole modes ($k = 1$) with one period of density modulation are observed. This corresponds to transverse displacements of the beam. The quadrupole modes ($k = 2$) corresponding to coherent beam width oscillations only interact very weakly with the vacuum chamber environment. The situation is different for very localised interactions such

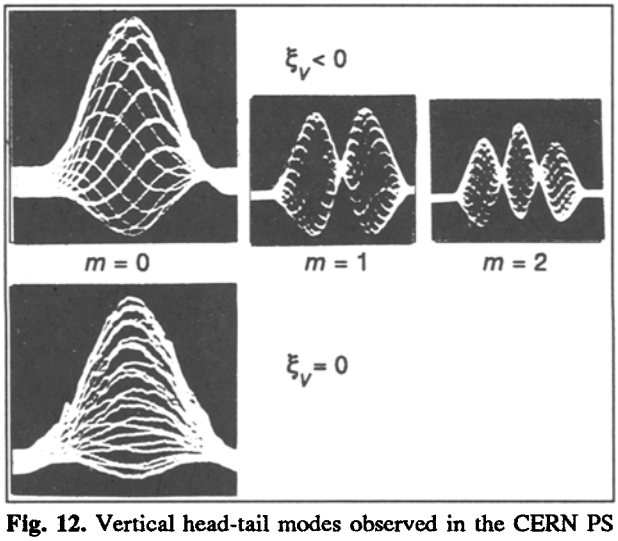


**Fig. 12.** Vertical head-tail modes observed in the CERN PS Booster.

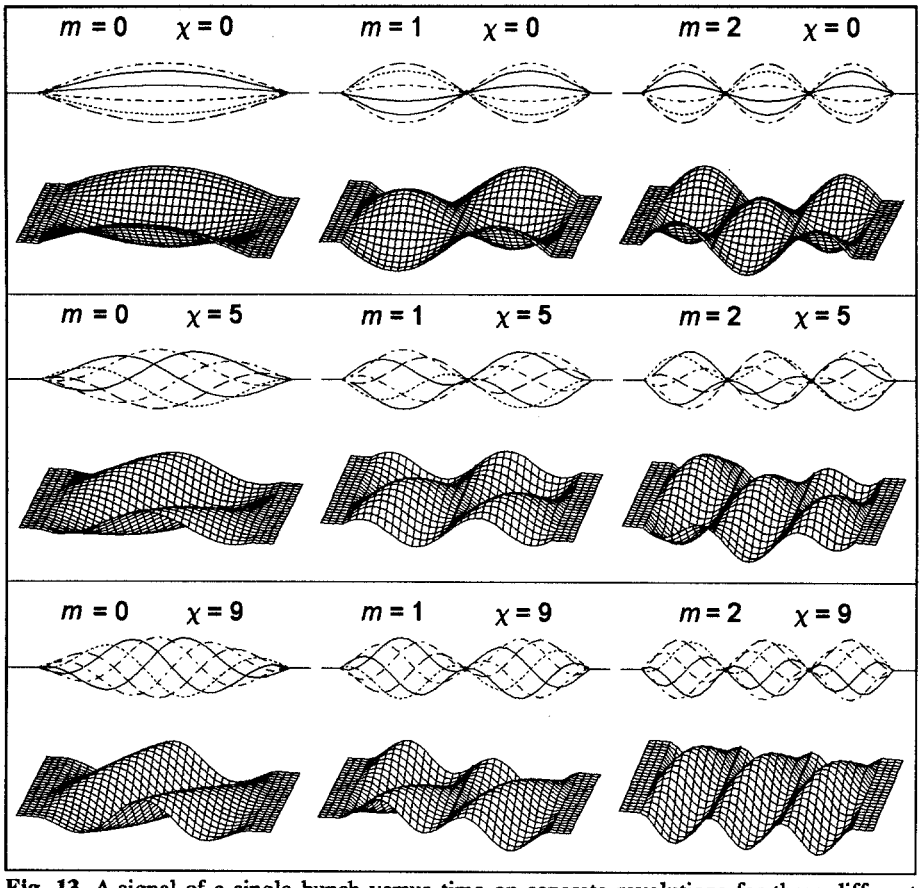


**Fig. 13.** Δ-signal of a single bunch versus time on separate revolutions for three different chromaticities, modes $m = 0, +1, +2$. Upper traces: every fourth turn, superimposed. Lower traces: every turn, mountain range display. Fractional tune: $q = 0.0417$, 15° phase advance per turn.

as coherent beam-ion [22] and coherent beam-beam interactions [23][24]. Transverse coherent beam-ion quadrupolar instabilities have been observed with coasting antiproton beams in the CERN AA [25], and can be expected to occur for bunched beams as well. A quadrupolar pick-up is required to observe such modes.

By taking the Fourier transform of the average transverse displacement times the bunch current (the signal seen by the Δ-signal of a transverse pick-up for dipole modes $k = 1$), we get the frequency spectrum of the modes. It is a line spectrum, and the line frequencies for mode $(n, m, k)$ are:

$$f_{nmk,p} = (n + pM + kQ) f_0 + m f_s \quad -\infty < p < \infty \tag{12}$$

where $f_0$ is the revolution frequency, $f_S$ is the synchrotron frequency, and $p$ is an integer assuming both negative and positive values. It is convenient from a

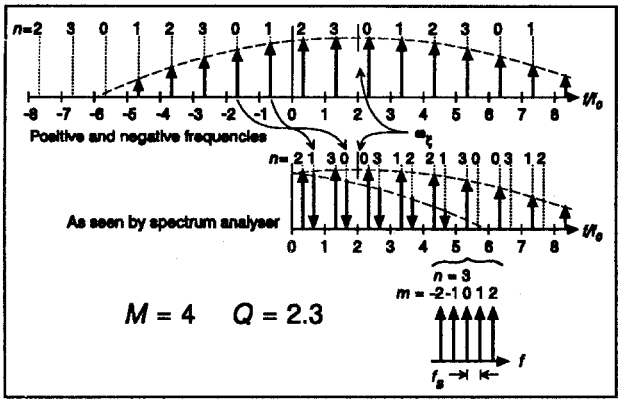


**Fig. 14.** The line spectrum of transverse bunched-beam modes

mathematical point of view to let the frequencies $f_{nmk,p}$ assume both positive and negative values, although physically a frequency is always a positive quantity.

This line spectrum is depicted graphically for dipole modes ($k = 1$) on Fig. 14, where the mode lines originating from negative values of $f_{nmk,p}$ are shown as downward pointing arrows, while mode lines originating from positive values are shown pointing up. Each betatron line splits up into several lines corresponding to the different within-bunch mode numbers $m$ and separated by the synchrotron frequency as given by equation (12) and shown on Fig. 14. The envelope shown corresponds to mode $m = 0$. These spectral lines are those associated with the coherent motion of the bunches. In practice the beam will never pass exactly through the electrical centre of the pick-up, and additional lines associated with the stationary bunch spectrum will be observed, like the bunch frequency $Mf_0$ and harmonics thereof.

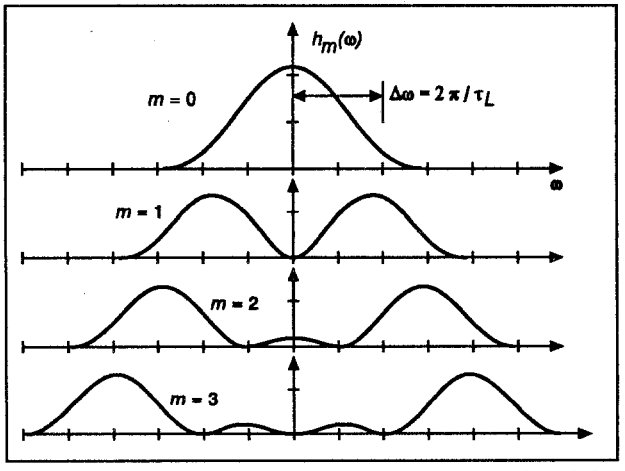


**Fig. 15.** Power-spectrum envelopes for modes m = 0 to 3 for zero chromaticity.

Each bunched-beam mode *(m,n)* has thus two lines appearing within each band $Mf_0$ wide between two bunch frequency harmonics, one pointing up and one pointing down. Each mode has therefore a large number of spectral lines.

The envelope or the relative amplitude of those lines depends upon the within-bunch mode number $m$, the bunch length $\tau_L$, and the chromaticity $\xi$. The power spectrum envelopes $h_m(\omega)$ for zero chromaticity are shown on Fig. 15. The width of the envelope is inversely proportional to the bunch length $\tau_L$. The chromaticity $\xi$ will shift the centre frequency of those envelopes to the chromatic frequency $\omega_\xi$ given by:

$$\omega_\xi = \frac{\xi}{\eta} Q\omega_0 = \chi / \tau_L \tag{13}$$

where all symbols have been defined previously.

### 5.1 Sacherer's Formula for Transverse Bunched-Beam Modes

Due to electromagnetic interactions with the beam environment quantitatively described by the transverse coupling impedance $Z_T(\omega)$, the coherent mode frequencies are shifted a complex quantity $\Delta\omega_{mn}$ away from their low-intensity values. This shift is obtained by a weighted sum ($h_m(\omega)$) of the coupling impedance $Z_T(\omega_p)$ sampled at all those frequencies that corresponds to a mode line (see Fig. 14, equation (12)) of mode $(m,n)$, Sacherer's formula [20][21]:

$$\Delta\omega_{m,n} = \frac{1}{m+1} \frac{je\beta I_0}{2Q\omega_0 \gamma m_0 L} \frac{\sum_p Z_T(\omega_p) h_m(\omega_p - \omega_\xi)}{\sum_p h_m(\omega_p - \omega_\xi)} \tag{14}$$

where $\beta$ and $\gamma$ are the usual relativistic parameters, $e$ the electron charge, $m_0$ the particle rest mass, $I_0$ the current per bunch and $Z_T$ the transverse coupling impedance in ohms/m.

The *growth rate* of mode $(m,n)$ is $-\mathrm{Im}\{\Delta\omega_{mn}\}$ which is related to the *real* part of the coupling impedance $Z_T(\omega)$. The *real coherent frequency shift* of mode $(m,n)$ is $\mathrm{Re}\{\Delta\omega_{mn}\}$, which is related to the *imaginary* part of the coupling impedance.

### 5.2 Discussion of Sacherer's Transverse Bunched-Beam Formula

The real part of the transverse coupling impedance has odd symmetry: $\mathrm{Re}\{Z_T(\omega)\} = -\mathrm{Re}\{Z_T(-\omega)\}$ and $\mathrm{Re}\{Z_T(\omega)\} > 0$ for $\omega > 0$ for passive impedances. The negative mode lines contribute therefore to growth in (14) while the positive mode lines contribute to damping. For zero chromaticity there is therefore cancellation of positive and negative frequency contributions for broad-band impedances and resonant impedances with bandwidths larger than the bunch frequency $Mf_0$ (decay time less than the bunch separation) similarly to the longitudinal case.

For non-zero chromaticity the cancellation for broad-band impedances is no longer effective, as the power spectrum envelopes $h_m(\omega - \omega_\xi)$ are shifted in frequency by $\omega_\xi$. For the naturally negative chromaticity above transition $\omega_\xi$ is negative, so all coupled-bunch modes $n$ are driven unstable by the real part of the broad-band (short range) coupling impedance. This is the so-called "head-tail" effect and is a single-bunch effect proportional to the current per bunch. This effect can also be used with advantage to damp the instabilities by correcting the chromaticity to a positive value thus achieving a passive damping of all bunches and thus all coupled-bunch modes.

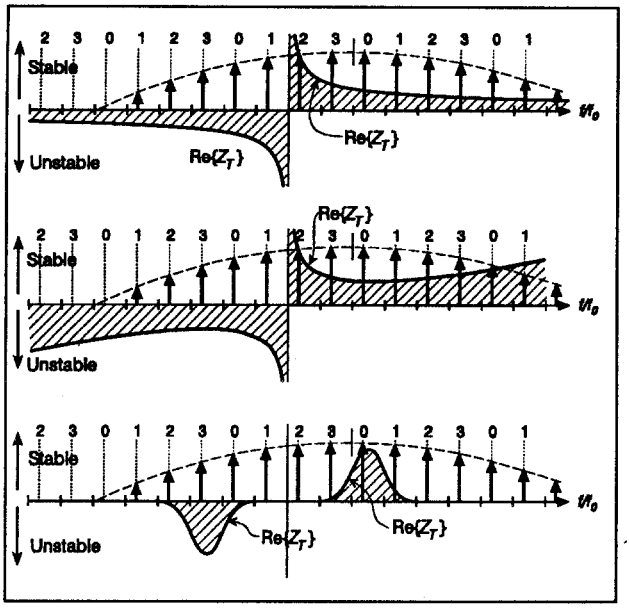


**Fig. 16.** Mode spectra for mode $m = 0$ and positive chromaticity (above transition) for typical examples of transverse coupling impedances with long-range wake. Top: Thick-wall, resistive-wall impedance; middle: same plus broad-band, high-frequency, coupling impedance; bottom: resonant narrow-band impedance.

For resonant impedances with bandwidths smaller than the bunch frequency $Mf_0$ (decay time longer than bunch separation), a single mode line for each mode dominates in the sum and one or several coupled-bunch modes are growing. The growth rate is proportional to the total current $I$ in $M$ bunches, and independent of the number of bunches unless the bunch frequency is low enough to get partial cancellation from another mode line of the same mode falling within the resonator bandwidth.

Some typical examples to illustrate this folding of the mode line spectrum with the frequency response of the coupling impedance are shown on Fig. 16 for a slightly positive chromaticity. On the top figure the long-range wake from the resistive-wall impedance drives the $n = 1$, $m = 0$ mode unstable, on the middle figure this mode is stabilised by the broad-band (single-bunch) interaction with the high-frequency impedance thanks to a positive $\omega_\xi$. On the bottom figure a narrow-band resonator drives the $n = 3$, $m = 0$ mode unstable.

For a low number of bunches $M$ the damping effect due to the head-tail effect and a positive chromaticity (above transition) may be effective in damping multibunch instabilities. This is much less so for large $M$ as the damping effect is proportional to the single-bunch current while the growth rate due to a long-range wake (resistive wall or resonator) is proportional to the total circulating current.

## 5.3 Transverse Mode Coupling

In the transverse case the imaginary part of $Z_T$ has even symmetry, $\mathrm{Im}\{Z_T(\omega)\} = \mathrm{Im}\{Z_T(-\omega)\}$, so contributions to the sum in (14) from positive and negative mode lines add up and give a real coherent frequency shift. Since $h_0(\omega)$ samples low frequencies with a predominantly inductive impedance while $h_1(\omega)$ samples much higher frequencies where the reactance may become capacitive, the

real coherent shift of the $m = 0$ modes is different from the real coherent shift of the $m = \pm 1$ modes, in particular if the bunch length is short relative to the vacuum chamber. When the difference in frequency shift of the $m = 0$ mode and the $m = -1$ mode is equal to their separation by the synchrotron frequency, the two mode frequencies merge together. If this threshold is exceeded they become imaginary, an instability known as the fast head-tail or transverse mode coupling instability occurs [26][27]. It is a single-bunch instability since it is due to the broad-band or short-range wake characteristics of the transverse coupling impedance. It is often an intensity limiting factor for large rings with few short bunches.

## 6 Transverse Coupling Impedances

As in the longitudinal case coupling impedances can be subdivided into short-range wake or broad-band impedances and long-range wake or narrow-band impedances, depending on whether the bandwidth is larger or smaller than the bunch frequency $Mf_0$. The transverse coupling impedance $Z_T$ (for dipolar modes, $k = 1$) is defined as the integral over one turn of the combined electric and magnetic deflecting field divided by the current $I$ times displacement $\Delta$, giving:

$$Z_T = j\frac{\oint\left[\overline{E}+\overline{v}\times\overline{B}\right]_{\perp} ds}{\beta I \Delta} \quad \text{[ohms / meter]} \tag{15}$$

where $\beta = v/c$, $c$ is the speed of light, and $\perp$ indicates the component perpendicular to the beam direction.

### 6.1 Resistive-Wall Impedance

For frequencies where the skin depth $\delta$:

$$\delta = \sqrt{\frac{2\rho}{\mu_0 \omega}} \tag{16}$$

is smaller then the vacuum chamber thickness, the surface resistivity $R_{surf}$ in ohms per square is given by:

$$R_{surf} = (1+j)\rho/\delta = (1+j)\sqrt{\frac{\mu_0 \rho \omega}{2}} \tag{17}$$

where $\rho$ is the specific resistivity of the chamber material and $\mu_0 = 4\pi\ 10^{-7}$ is the permeability of free space. The longitudinal coupling impedance due to the surface resistivity is simply the aspect ratio of the vacuum chamber surface times the surface resistivity:

$$Z_L = \frac{2\pi R}{2\pi b} R_{surf} = \frac{R(1+j)}{b}\sqrt{\frac{\mu_0 \rho \omega}{2}} \tag{18}$$

where b is the vacuum chamber radius. It can be shown that for a circular chamber the following relation holds between the longitudinal and transverse coupling impedances:

$$Z_T(\omega) = \frac{2Z_L(\omega)c}{b^2\omega} \tag{19}$$

where c is the speed of light. From this equation it is seen that since $\mathrm{Re}\{Z_L\}$ is an even and $\mathrm{Im}\{Z_L\}$ an odd function of $\omega$, the opposite will be true for the transverse coupling impedance: $\mathrm{Re}\{Z_T\}$ has odd symmetry (as depicted on Fig. 16) and $\mathrm{Im}\{Z_T\}$ has even symmetry. It also follows from equations (16), (17) and (18), that the real part of the transverse coupling impedance scales as $\omega^{-1/2}$, such that the coupled-bunch mode with a negative mode line frequency closest to the origin is driven unstable.

While the transverse resistive wall impedance can be extremely harmful due to the singularity near the origin, the longitudinal resistive wall impedance (17) is generally harmless since the mode $m = 0$ does not exist in the longitudinal case and the longitudinal form factor (7) for the lowest mode $m = 1$ scales as $\omega^2$ at low frequencies. In the transverse case, even modes with $m \neq 0$ can be driven unstable by the resistive-wall impedance as non-zero chromaticity shifts the mode spectrum envelopes such that they overlap with the origin.

The resistive-wall impedance is particularly harmful for large rings with high current like PEP II, SSC and LHC. The frequency of the lowest frequency transverse mode line is very low, the aspect ratio of the vacuum chamber surface is high, and the beam current is high. For LHC it is a serious problem even with a very low resistivity, copper-coated, vacuum chamber at cryogenic temperatures.

## 6.2 Parasitic Higher-Order Modes

As in the longitudinal case the RF cavities are often the major source of long-range, narrow-band coupling impedances due to undesired higher-order deflecting modes. As in the longitudinal case two effects contribute to make these particularly harmful in high-current colliders, namely the *high current and the high bunch frequency.*

For low bunch frequencies not much HOM damping is required before the HOM bandwidth becomes comparable to the bunch frequency, in which case *any coupled-bunch mode n* will have at least one positive and at least one negative frequency contribution to the sum in equation (14), of which the stabilising terms will dominate provided the chromaticity has the proper sign. For high bunch frequencies positive and negative contributions in (14) from the same mode *n* may be widely separated (up to $Mf_0/2$), and unstable coupled-bunch modes are driven unstable in spite of applying a positive chromaticity above transition.

## 7 Damping of Multibunch Instabilities

For moderate total currents (say 100 mA to 1 A), aggressive HOM damping of transverse and longitudinal modes in the RF cavities may keep the multibunch growth rates below the synchrotron radiation threshold. The resistive-wall instability is easier to damp if a tune just above an integer is used. Additional damping by the head-tail effect can be obtained by a positive chromaticity above transition, especially if the number of bunches is not too large. The longitudinal $n = M$-1 mode driven by the detuned fundamental RF resonance is normally not a problem except for very large rings (example SSC) or very low RF voltages.

For very high currents (for example LHC, PEP II, KEK B-factory) in the order of one ampere or more, all four sources (transverse: resistive-wall and HOM's, longitudinal: HOM's and detuned fundamental RF resonance) of multibunch instabilities cause growth rates in excess of synchrotron and/or Landau damping rates. In this case *longitudinal and transverse multibunch feedback systems* [3][28-33] become essential to maintain stability.

Full bandwidth (all coupled-bunch modes, bunch-by-bunch feedback for example) transverse dampers can in addition be used to raise the transverse mode coupling threshold. This is achieved by phasing it in such a way that it represents a *reactive impedance* which gives a real frequency shift of the $m = 0$ modes, which compensates the shift of the $m = 0$ modes from the broad band transverse machine impedance [34].

The detuned fundamental RF resonance produces such a fast growth rate that it becomes essential to first reduce the apparent cavity impedance by *local RF feedback* [16][17][18] to bring the impedance down to a level where the residual growth rate can be dealt with by means of multibunch feedback.

## Conclusion

Colliders in the 70's and 80's typically had unseparated orbits, low number of bunches and therefore low bunch frequencies and were approaching single-bunch current limits. Short-range wake fields dominated the limiting phenomena: space-charge tune shift, beam-beam tune shift, transverse mode coupling and turbulent bunch lengthening. Examples are CESR, SPEAR, PEP SppS collider and the Tevatron collider.

The high-luminosity, two-ring colliders of the next decade (like PEP II, CESR B, KEK B-factory, $\tau$/c factories, DAFNE, SSC, LHC) have very high bunch frequencies and high total beam currents. In addition to pushing single-bunch limits, multibunch instabilities and long-range wake fields will become important limiting phenomena. RF cavity feedback, aggressive HOM damping, and longitudinal and transverse multibunch feedback systems will become essential to achieve the specified design goals.

## References


[1] F.J. Sacherer, A Longitudinal Stability Criterion for Bunched Beams, IEEE Trans. Nucl. Sci., NS-20, 825 (1973).

[2] F.J. Sacherer, Bunch Lengthening and Microwave Instability, IEEE Trans. Nucl. Sci., NS-24, 1393 (1977).

[3] F. Pedersen and F.J. Sacherer, Theory and Performance of the Longitudinal Active Damping System for the CERN PS Booster, IEEE Trans. Nucl. Sci., NS-24, 1396 (1977).

[4] F.J. Sacherer, Methods for Computing Bunched-beam Instabilities, CERN/SI-BR/72-5, (1972).

[5] G. Besnier, Contribution à la Théorie de la Stabilité des Oscillations Longitudinales d'un Faisceau Accéléré en Régime de Charge d'espace, Thesis, Université de Rennes, B-282, (1978).

[6] S. Hansen, H.G. Hereword, A. Hofmann, K. Hübner and S. Meyers, Effects of Space Charge and Reactive Wall Impedance on Bunched Beams, IEEE Trans. Nucl. Sci., NS-22, 1381 (1975).

[7] D. Boussard, Observations of Microwave Longitudinal Instabilities in the CERN PS, CERN Lab. II/RF/Int. 75-2 (1975).

[8] E. Keil and W. Schnell, Concerning Longitudinal Stability in the ISR, CERN-ISR-TH-RF/69-48 (1969).

[9] E. Haebel, RF Design (Higher-order Modes), these proceedings.

[10] P. Arcioni, and G. Conciauro, Feasibility of HOM-free Accelerating Resonators: Basic Ideas and Impedance Calculations, Particle Accelerators, Vol. 36, 177 (1991).

[11] R. Rimmer, M. Allen, J. Hodgeson, K. Ko, N. Kroll, G. Lambertson, R. Pendleton, H. Schwarz, and F. Voelker, An RF cavity for the B-factory, Proc. 1991 IEEE Part. Acc. Conf., San Francisco, 819 (1991).

[12] H. Padamsee, P. Barnes, C. Chen, W. Hartung, H. Hiller, J. Kirchgessner, D. Moffat, R. Ringrose, D. Rubin, Y. Samed, D. Saraniti, J. Sears, Q. S. Shu, and M. Tigner, Accelerating Cavity Development for the Cornell B-factory, CESR-B. Proc. 1991 IEEE Part. Acc. Conf., San Francisco, 786 (1991).

[13] Y. Chao, P.L. Corredoura, A. Hill, P. Krejcik, T. Limberg, M. Minty, M. Nordby, F. Pedersen, H. Schwarz, W.L. Spence, P.B. Wilson, Damping The pi Mode Instability in the SLC Damping Rings With a Passive Cavity, SLAC-PUB-5868, (1992) and Proc. 15th Int. Conf. on High-Energy Accelerators, Hamburg, Germany, Jul 20-24, (1992).

[14] K.W. Robinson, Stability of Beam in Radiofrequency System, CEA Report CEAL-1010, (1964).

[15] D. Boussard, RF Power Requirements for a High Intensity Proton Collider, Proc. 1991 IEEE Part. Acc. Conf., San Francisco, 2447 (1991).

[16] D. Boussard, Control of Cavities with High Beam Loading, IEEE Trans. Nucl. Sci. NS-32, 1852 (1985).

[17] F. Pedersen, A Novel RF Cavity Tuning Feedback Scheme for Heavy Beam Loading, IEEE Trans. Nucl. Sci. NS-32, 2138 (1985).

[18] F. Pedersen, RF Cavity Feedback, CERN/PS 92-59 (RF), and Proceedings of B factories, The State of the Art in Accelerators, Detectors and Physics, SLAC-400, 192 (1992).

[19] T. Shintake, Proposal of Accelerating RF-cavity Coupled with an Energy Storage Cavity for Heavy Beam Loading Accelerators, KEK Preprint 92-191.

[20] F.J. Sacherer, Transverse Bunched Beam Instabilities - Theory, Proc. 9th International Conference on High Energy Accelerators, Stanford, 347 (1974).

[21] F.J. Sacherer and B. Zotter, Transverse Instabilities of Relativistic Particle Beams in Accelerators and Storage Rings, CERN 77-13, 175 (1977).

[22] R. Alves Pires, D. Möhl, Y. Orlov, F. Pedersen, A. Poncet, S. van der Meer, On the Theory of Coherent Instabilities due to Coupling Between a Dense Cooled Beam and Charged Particles from the Residual Gas, Proceedings of the 1989 IEEE Particle Accelerator Conference, Chicago, 800 (1990).

[23] A.W. Chao and R.D. Ruth, Coherent Beam-beam Instability in Colliding Beam Storage Rings, SLAC PUB 3400 (1984).

[24] K. Hirata and E. Keil, Barycentre Motion of Beams due to Beam-beam Interaction in Asymmetric Ring Colliders, Proceedings of 2nd EPAC, Nice 1990.

[25] G. Carron, D. Möhl, Y. Orlov, F. Pedersen, A. Poncet, S. van der Meer, D.J. Williams, Observation of Transverse Quadrupole Mode Instabilities in Intense Cooled Antiproton Beams in the AA, Proceedings of the 1989 IEEE Particle Accelerator Conference, Chicago, 803 (1990).

[26] R.D. Kohaupt, Transverse Instabilities in PETRA, Proc. 11th Int. Conf. on High Energy Accelerators, Geneva 1980, 562 (1980).

[27] B. Zotter, Transverse Instabilities ue to Wall Impedances in Storage Rings, IEEE Trans. Nuclear Sci., NS-32, 2191 (1985).

[28] T. Kasuga, M. Hasumoto, T. Kinoshita and H. Yonehara, Longitudinal Active Damping System for UVSOR Storage Ring, Japanese Journal of Applied Physics, Vol. 27, No. 1, January, 100 (1988).

[29] D. Briggs, J.D. Fox, W. Hosseini, L. Klaisner, P. Morton, J.L. Pellegrin and K.A. Thompson, Computer Modelling of Bunch-by-bunch Feedback for the SLAC B-factory Design, Proc. 1991 IEEE Part. Acc. Conf., San Francisco, 1407 (1991).

[30] D. Briggs, P. Corredoura, J.D. Fox, A. Gioumousis, W. Hosseini, L. Klaisner, J.L. Pellegrin, K.A. Thompson, and G. Lambertson, Prompt Bunch by Bunch Synchrotron Oscillation Detection via a Fast Phase Measurement, Proc. 1991 IEEE Part. Acc. Conf., San Francisco, 1404 (1991).

[31] L. Vos, Transverse Feedback System in the CERN SPS, CERN SL/91-40 (1991)

[32] M. Ebert, D. Heins, J. Klute, R.D. Kohaupt, K.H. Matthiesen, J. Meinen, H. Musfeldt, S. Pätzold, K.H. Richter, J. Rümmler, H.P. Scholz, M. Schweiger, M. Sommerfeld, J. Theiss, Transverse and Longitudinal Multi-Bunch Feedback Systems for PETRA, DESY 91-036 (1991).

[33] F. Pedersen, Feedback Systems, CERN PS/90-49 (AR) (1990).

[34] S. Myers, Stabilization of the Fast Head-tail Instability by Feedback, Proceedings of the 1987 IEEE Particle Accelerator Conference, Washington, 503 (1987).